ELSEVIER

Energy and Buildings 1300 (2000) 1–13

ENERGY AND BUILDINGS

www.elsevier.com/locate/enbuild

Advanced control strategy of a solar domestic hot water system with a segmented auxiliary heater

T. Prud'homme*, D. Gillet

Institut d'automatique, École Polytechnique Fédérale de Lausanne, CH-1015 Lausanne, Switzerland

Abstract

This paper describes improvements that can be introduced at both a structural and control level in order to improve the overall efficiency of solar kits for domestic hot water supply.

The plant under consideration is a solar domestic hot water system (SDHWS) manufactured in Switzerland. The heat exchanger is a mantle, which surrounds the entire storage tank.

One major structural improvement has been designed. It consists of the replacement of one single electrical element as an auxiliary heater by three smaller ones with different lengths. This configuration requires the manipulation of two additional actuators. An advanced control strategy has been developed to handle the resulting complexity and to achieve higher performances. The actuators are the pump driving the fluid in the collector loop and the three electrical elements. A predictive control strategy has been proposed and validated. It requires solving of an optimization problem and implementation of a state estimator.

Weather forecasts as well as prediction of the users' needs in terms of tapped water are required to implement this predictive control strategy. The weather forecasts are provided on-line by the Swiss Meteorological Institute (SMI). The prediction of the users' needs is updated every day using an extended Kalman filter.

Segmentation of the auxiliary heater coupled with a suitable advanced control strategy have led to significant improvements in terms of comfort and energy consumption. © 2000 Elsevier Science B.V. All rights reserved.

Keywords: Domestic hot water supply; Auxiliary heater; Solar kit

1. Introduction

The current control strategies in solar domestic hot water system (SDHWS) are mainly based on manufacturers' know-how. However, these strategies do not take into account the evolution of the operational conditions, typically the users' needs in terms of draw-off and the weather conditions. They have been designed to work in the worst case scenario, often leading to very conservative behavior.

The initial goal of this contribution was the development of an advanced control strategy for all the variables manipulated. At this time, no changes in the design of the SDHWS were planned. However, previous results [1] have shown the potential benefit of implementing a segmented auxiliary heater.

The SDHWS and its model are described in Section 2. The segmentation of the auxiliary heater is detailed and justified in Section 3. The principle of the advanced control strategy is presented in Section 4. The optimization procedure and the state estimator are described in Sections 5 and 6, respectively. Section 7 presents how the predictions of weather data and the predictions of the users' needs in terms of draw-off are obtained. Simulation results and comparisons of the energy performance achieved with the advanced control strategy proposed versus a conventional one are given in Section 8.

2. The SDHWS and its dynamic model

A schematic view of the SDHWS under consideration is given in Fig. 1.

In this figure, the location of eight available temperature measurements M_i is indicated. Stratification in the storage tank is well established owing to four valves controlled by an autonomous switching law. Only one valve is opened at a time. The first valve (the highest one) is opened if $(M_8 - M_2) > 0$, the second is opened if $(M_8 - M_2) > 0$ and $(M_8 - M_3) > 0$, etc. Basically, a valve is opened if the temperature of the collecting fluid at the output of

* Corresponding author.
E-mail address: thierry.prudhomme@epfl.ch (T. Prud'homme).

0378-7788/00/$ – see front matter © 2000 Elsevier Science B.V. All rights reserved.
PII: S0378-7788(00)00107-9

UNCORRECTED PROOF

Nomenclature

State variables of the SDHWS model

T_c	temperature of the liquid inside the collector (K)
$T_{h,j}$	temperature of the jth node of the heat exchanger (K)
$T_{p,k}$	temperature of the kth node of the pipe of the collector loop (K)
$T_{s,i}$	temperature of the ith node of the store (K)

Constant parameters of the SDHWS model

A	collector area (m^2)
c_0	collector's optical efficiency
c_1	collector's heat loss coefficient ($kJ/(m^2K)$)
C_{col}	thermal capacity of the collector (kJ/K)
C_{pc}	specific thermal capacity of the collecting fluid (kJ/(kgK))
C_{pf}	specific thermal capacity of the fluid in the store (kJ/(kgK))
$K_{h,a}$	heat loss capacity rate from the heat exchanger to ambient (kW/K)
$K_{h,s}$	heat transfer capacity rate from the heat exchanger to the store (kW/K)
$K_{p,a}$	heat loss capacity rate from the pipe of the collector loop to ambient (kW/K)
$K_{s,a}$	heat loss capacity rate from the store to ambient (kW/K)
$M_{h,j}$	mass of the jth node of the heat exchanger (kg)
$M_{p,k}$	mass of the kth node of the pipe of the collector loop (kg)
$M_{s,i}$	mass of the ith node of the store (kg)

Manipulated inputs

$\dot{m}_C$	mass flow rate of the collecting fluid (kg/s)
P_1	power supply of the longest electrical element (kW)
P_2	power supply of the medium electrical element (kW)
P_3	power supply of the shortest electrical element (kW). It should be noted that $\dot{Q}_i$ and P_j are related. We have $\sum_{\text{all } i}\dot{Q}_i = P_1 + P_2 + P_3$
$\dot{Q}_i$	auxiliary heater input of the ith node of the store (kW)

Meteorological disturbances

I_T	global solar radiation on the collector surface (kW/m^2)
$T_{amb,ex}$	ambient temperature around the collector (K)
$T_{amb,in}$	ambient temperature around the store (K)

Other disturbances

$\dot{m}_L$	mass flow rate of the fluid in the store (kg/s)
T_{in}	temperature of the liquid at the input of the store (K)

Objective function

J	objective function
P_{elec}	power supplied to the three electrical elements (kW)
P_{pump}	power supplied to the pump driving the collecting fluid (kW)
P_{sol}	power gathered by the collector (kW)
α	trade-off factor between energy consumption and comfort

Optimization procedure

a	vector containing all of the decision variables a_i
a^0	initial choice for a
a^*	optimal choice for a
g_i	gradient of J versus a_i
G	vector containing all of the g_i
N	number of decision variables
x	vector containing the 28 temperatures of the model

Energy balance

E_{amb}	energy loss to ambient (kJ)
E_{elec}	electrical energy consumed by the auxiliary heaters (kJ)
E_{load}	energy tapped by the users (kJ)
E_{sol}	solar energy gathered (kJ)
ΔE	internal energy variation (kJ)
F_1	solar fraction computed in the common way (%)
F_2	solar fraction computed in the new way (%)

the collector is higher than the temperature in the storage tank at the level of this valve, and if no upper valve can be opened.

The storage, the mantle, the pipes of the collector loop and the collector are modeled using 13, 10, 4 and 1 node(s), respectively. In reality, the temperature of the water inside the storage tank and inside the heat exchanger vary gradually. This simple model, although detailed enough, is in fact well suited to develop and analyze control strategies without cumbersome computational limitations.

The dynamic behavior of the SDHWS is defined by computing the energy balance of each node. It leads to one differential equation per node. Using the conditional factor ξ_i (which enables or disables the corresponding term according to the node location), the energy balance is represented by Eq. (1) for each node (s,i) of the store, by Eq. (2) for each node (h,j) of the heat exchanger and, by Eq. (3) for the node (c) of the collector and by Eq. (4) for each node (p,k) of the pipes of the collector loop.

$$M_{s,i}C_{pf}\frac{dT_{s,i}}{dt} = \xi_i K_{h,s}(T_{h,i-2} - T_{s,i}) + \dot{m}_L C_{pf}(T_{s,i+1} - T_{s,i}) + (1-\xi_i)K_{s,a}(T_{amb,in} - T_{s,i}) + \dot{Q}_i \quad (1)$$

UNCORRECTED PROOF

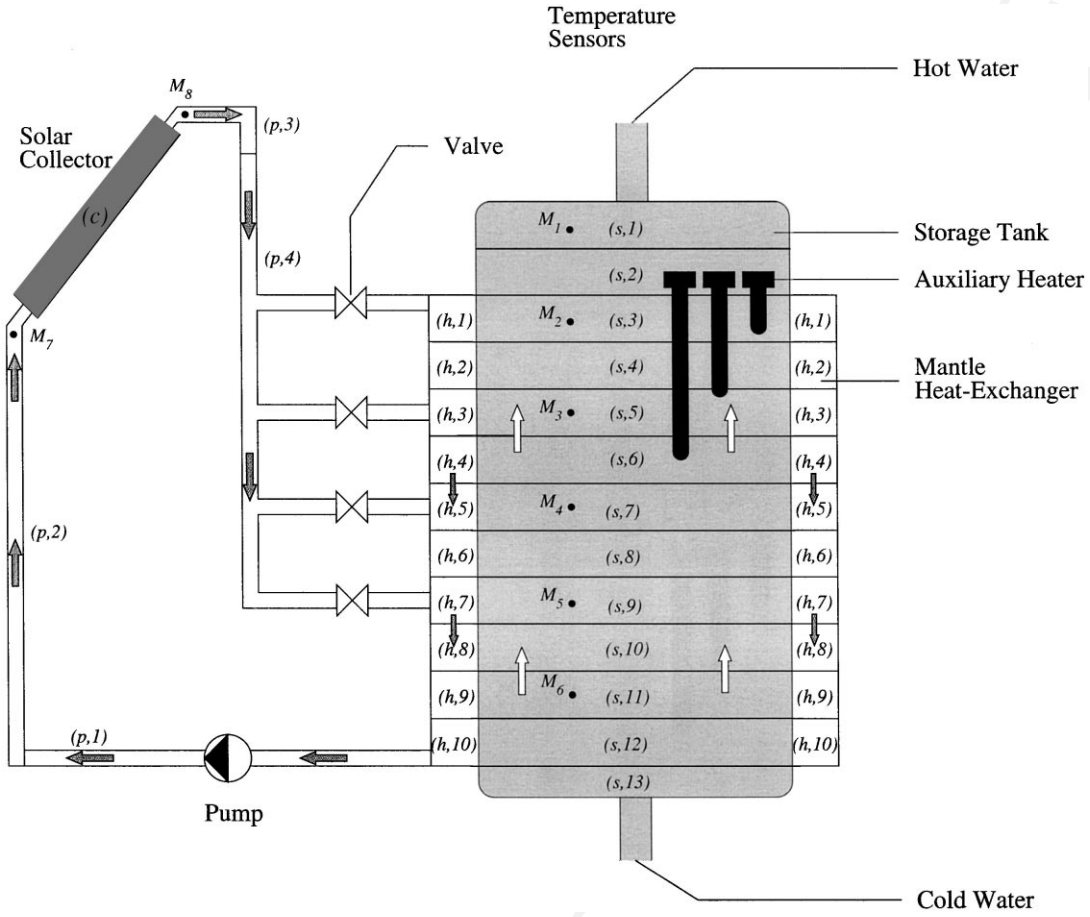


Fig. 1. The SDHWS and its division into nodes for modeling.

where

$i = \{1, \ldots, 13\}, \quad T_{s,14} = T_{\text{in}},$

$\xi_i = 1$ if $i \in \{3, \ldots, 12\}$, otherwise $\xi_i = 0.$

$$M_{h,j} C_{pc} \frac{\mathrm{d}T_{h,j}}{\mathrm{d}t} = K_{h,s}(T_{s,j+2} - T_{h,j}) + \dot{m}_{\text{C}} C_{pc}(T_{\text{test}} - T_{h,j}) + K_{h,a}(T_{\text{amb,ex}} - T_{h,j}) \quad (2)$$

where

$j = \{1, \ldots, 10\}$

and

$T_{\text{test}} = T_{h,j}$, if the opened valve is below the jth node
$T_{\text{test}} = T_{p,4}$, if the opened valve is at the same level as the jth node
$T_{\text{test}} = T_{h,j-1}$, if the opened valve is above the jth node

$$C_{\text{col}} \frac{\mathrm{d}T_{\text{c}}}{\mathrm{d}t} = c_0 A I_{\text{T}} - c_1 A(T_{\text{c}} - T_{\text{amb,ex}}) + \dot{m}_{\text{C}} C_{pc}(T_{p,2} - T_{\text{c}}) \quad (3)$$

$$M_{p,1} C_{pc} \frac{\mathrm{d}T_{p,1}}{\mathrm{d}t} = \dot{m}_{\text{C}} C_{pc}(T_{h,10} - T_{p,1}) + K_{p,a}(T_{\text{amb,in}} - T_{p,1})$$
$$M_{p,2} C_{pc} \frac{\mathrm{d}T_{p,2}}{\mathrm{d}t} = \dot{m}_{\text{C}} C_{pc}(T_{p,1} - T_{p,2}) + K_{p,a}(T_{\text{amb,ex}} - T_{p,2})$$
$$M_{p,3} C_{pc} \frac{\mathrm{d}T_{p,3}}{\mathrm{d}t} = \dot{m}_{\text{C}} C_{pc}(T_{\text{c}} - T_{p,3}) + K_{p,a}(T_{\text{amb,ex}} - T_{p,3})$$
$$M_{p,4} C_{pc} \frac{\mathrm{d}T_{p,4}}{\mathrm{d}t} = \dot{m}_{\text{C}} C_{pc}(T_{p,3} - T_{p,4}) + K_{p,a}(T_{\text{amb,in}} - T_{p,4}) \quad (4)$$

All the terms appearing in these equations are defined in the nomenclature.

3. Segmentation of the auxiliary heater

The auxiliary heater introduced in every SDHWS is essential to meet the requirements in terms of draw-off. However, a bad control strategy of this auxiliary heater may reduce the overall energy benefit by destroying the stratification and disabling the two upper valves. This is particularly true for the system considered, since its mantle heat exchanger surrounds almost the entire surface of the sto-

UNCORRECTED

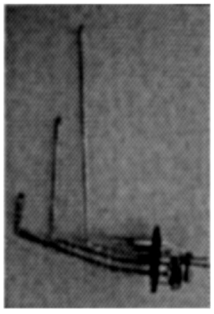


Fig. 2. The segmented auxiliary heater.

rage tank, including the part in which the auxiliary heater stands. To overcome the drawbacks of such a structure, an improvement has been designed. This consists of the replacement of the traditional single electrical element by three smaller ones with different lengths and can be seen from the schematic view in Fig. 1 as well as from the photo in Fig. 2.

Together, these new elements must supply the same power as the previous one, but may be activated independently according to both the expected load and the solar radiation. A combined auxiliary heater as proposed allows a better control of the amount of heated water in the upper part of the store and helps to preserve the stratification.

4. Predictive control principle

To achieve better overall performances, the controller has to take advantage of additional information such as the dynamic model of the system and the a priori knowledge of the most significant disturbances. In that way, the variables manipulated (inputs) can be adjusted according to a predicted behavior of the system until satisfactory performances are obtained. The resulting optimal inputs are then applied to the real plant. The performance level is characterized by an objective function that has to be minimized using a suitable optimization algorithm. A scheme illustrating this principle is given in Fig. 3.

The term *predictive* results from the fact that changes in the operational conditions are anticipated. For example, it can be understood intuitively that the auxiliary heaters will be turned on before each draw-off, thereby providing only the amount of energy required to satisfy the users' needs. An excellent review of this control strategy appears in [2]. Other related works have been done in the area of predictive control of passive and active solar systems [3–5].

As mentioned above, the performances desired are represented by an objective function. In this special case, the objective is twofold: the electrical consumption is minimized whereas the comfort of the users is maximized. The objective function chosen J, as used to carry out this optimization, is the following:

$$J = \int_{\text{one day}} \{[P_{\text{elec}} - (P_{\text{sol}} - P_{\text{pump}})] + \alpha(T_{s,1} - T_{\text{set}})^2\}\,\mathrm{d}t \tag{5}$$

where P_{elec} is the electrical consumption of the three auxiliary heaters, P_{sol} is the solar energy collected, P_{pump} the power required by the pump to drive the fluid in the collector loop and $T_{s,1}$ is the temperature in the upper part of the storage tank. The parameter α is a trade-off factor and T_{set} is the average temperature desired by the users. T_{set} has been chosen equal to 55°C. To summarize, this control strategy aims at minimizing the electrical consumption while keeping the temperature of the water going out from the tank as close as possible to the chosen T_{set}. This objective function is minimized over a 1-day horizon. Ideally, it should be minimized over the whole lifetime of the installation. However, because of obvious computation limitations, and because of the time-limited reliability of the weather forecasts, a 1-day horizon has been chosen. This justifies the fact that P_{sol} is introduced in this objective function. Indeed, over a long time, minimizing the electrical consumption or maximizing the solar energy collected is strictly equivalent. However, over the horizon chosen, they are not equivalent. Indeed, the variation of the internal energy is not negligible in a 1-day energy balance.

At this stage, it should be noted that no penalties have been added in the cost function to take into account the fact that electricity may be cheaper during day time than during the night. This can be done easily by multiplying P_{elec} in the cost function by a time-dependent term. In this paper, it is assumed that the electrical elements can be turned on during day time without any additional cost.

If P_1, P_2 and P_3 are the power supply of the longest, the medium and the shortest electrical elements, respectively, P_{elec} is described as follows:

$$P_{\text{elec}} = P_1 + P_2 + P_3 \tag{6}$$

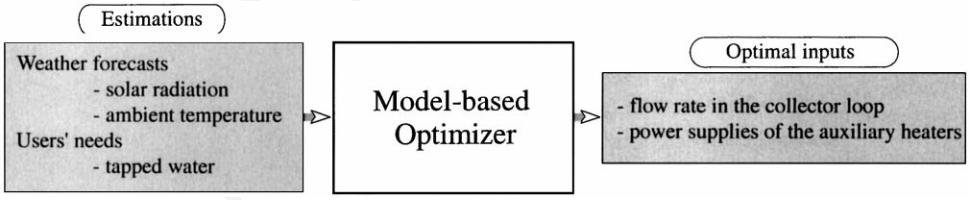


Fig. 3. Predictive control principle.

UNCORRECTED PROOF

P_{elec} is also obviously linked to the term Q_i that appears in Eq. (1). The relation between these two terms is the following:

$$\sum_{\text{all i}} \dot{Q}_i = P_{elec} \tag{7}$$

P_{sol} is given by

$$P_{sol} = \dot{m}_C C_{pc}(T_{p,3} - T_{p,2}) \tag{8}$$

P_{pump} is given by

$$P_{pump} = K\dot{m}_C^3 \tag{9}$$

where K is a constant taking into account the pressure losses in the collector loop and the efficiency of the pump.

The flow rate in the collector loop and the power supply of each electrical element are manipulated separately in order to minimize the objective function.

The flow rate can vary continuously between a lower and an upper bound whereas the power supplies can, depending on the configuration chosen, either take only two discrete values or also vary continuously between bounds. The optimization has been carried out in both cases to ease the comparison and justify the final implementation scheme.

5. Optimization procedure

The optimization algorithm used to minimize the objective function is quite simple. First, the inputs to be optimized are parameterized so as to transform the infinite dimensional problem into a finite dimensional one. There are two kinds of parameterizations, depending on the type of inputs. If the input can vary continuously, it is chosen piecewise continuous with a 20 min sampling period. In that case, the values of the input at each sampling time are optimized. If the input can take only two discrete values, a fixed sequence is chosen and the switching times are optimized. These two parameterizations are summarized in Fig. 4. The arrows indicate in which direction the curves are modified during the optimization procedure.

Thus, all the inputs are described by a finite number of variables called decision variables. These decision variables are denoted a_i and are grouped together in the vector a. a^0 and a^* represent the initial and the optimal choice, respectively. The latter is the one minimizing the objective function.

For conciseness, the 28 differential equations that form the dynamic model and the objective function given above are written as follows:

$$\dot{x} = f(x, u, p, v) \tag{10}$$

$$J = \int_{t_0}^{t_0+D} L(x, u, p, v)\, \mathrm{d}t \tag{11}$$

where x is the state vector containing the 28 temperatures (state variables) of the model, its elements x_i are the state variables, u is the vector containing the four inputs manipulated (flow rate in the collector loop and the power supply of the three electrical elements), p the vector containing all the constant parameters of the model and v the vector containing all the disturbances (weather forecasts and users' needs in terms of draw-off).

It is assumed that the optimization procedure is performed at time t_0 and covers a 1-day period (D). The vector p containing the constant parameters of the model is known, owing to an adequate identification procedure. All the disturbances contained in the vector v are estimated over the horizon $H = [t_0; t_0 + D]$, the related estimation procedure is described later. The value of u over H and of $x(t_0)$ are needed to solve numerically the set of differential equations (Eq. (10)).

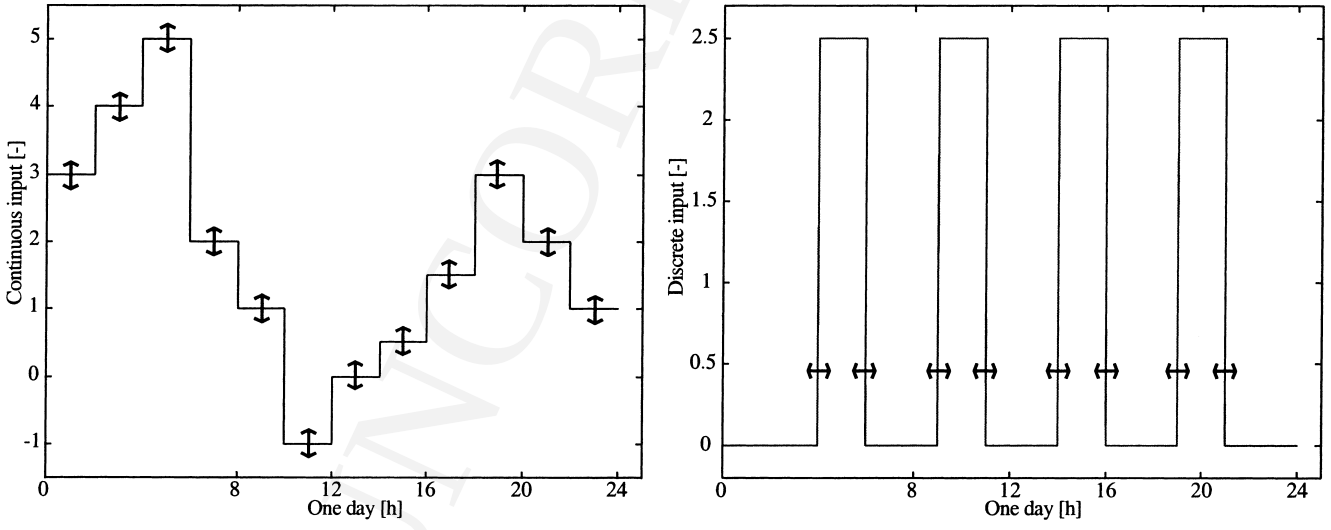


Fig. 4. Alternative parameterizations of the inputs.

UNCORRECTED PROOF

Given the parameterization previously described, u is completely defined by a. Therefore, given $x(t_0)$ and a set of decision variables a, x can be computed over H and, in the same way, the objective function J can be evaluated. Finally, if $x(t_0)$ is given, from an optimization point of view, the objective function J can be seen simply as a function of a.

The dimension of the vector a, which is also the number of decision variables, is called N. An initial guess a^0 for a has to be chosen to start the optimization. As the optimization problem is not convex, a^0 has to be chosen carefully. Then the algorithm computes a^1, a^2, $\ldots, a^k$, which verifies $J(a^0) > J(a^1) > J(a^2) \cdots > J(a^k)$. The procedure is stopped when the difference $J(a^{k+1}) - J(a^k)$ becomes small enough.

The algorithm used to perform this optimization is based on the gradient G of the objective function J versus a. In the present case, the elements g_i of G cannot be computed analytically. Thus, the perturbation method is chosen to estimate them numerically:

$$g_i = \frac{\partial J}{a_i}(a^k) \approx \frac{J(a^k + \varepsilon e_i) - J(a^k)}{\varepsilon} \tag{12}$$

where ε is a scalar chosen adequately to discriminate between cost variation and numerical rounding errors, and e_i the ith vector of the canonical basis of $\Re^N$.

The algorithm evaluates $N + 1$ times the objective function at each step, which means that the set of differential equations of (10) has to be solved $N + 1$ times. Therefore, it may induce a heavy computational load if the number of decision variables is chosen inadequately.

To avoid the computation of unrealistic values for the decision variables, such as a flow rate that the pump cannot afford, upper bounds $\overline{a}_i$ and lower bounds $\underline{a}_i$ of the decision variables a_i are also taken into account.

The way the algorithm implemented handles this type of constraint follows. If the ith decision variable hits one of its bound, then the ith element of the gradient of the objective function is taken as equal to zero. In fact, it is a special case of the projected gradient algorithm described in detail in [6]. If several variables hit their bound, the gradient is projected to the intersection of the hyper-planes defined by the constraints. In our special case, it is the same approach as taking the corresponding gradients of the objective function equal to zero.

Once G has been computed, the correction of the decision variables in the direction specified by the gradient has to be determined in order to reduce the objective function as much as possible. This is a one-dimensional problem that can be solved with the dichotomy, the Fibonacci or the golden section search. These well-known methods are described in [6]. The dichotomy method has proved to be suitable for the SDHWS.

Despite the fact that the decision variables are determined and can be applied over a 1-day horizon owing to the approach previously described, the measurements available can be used to regularly refine the optimum estimates. The feedback mechanism resulting reduces the effect of model mismatches and unforeseen disturbances. To implement this feedback mechanism, a state estimator has to provide an estimate $\hat{x}$ of x owing to the only eight measurements available grouped together in y.

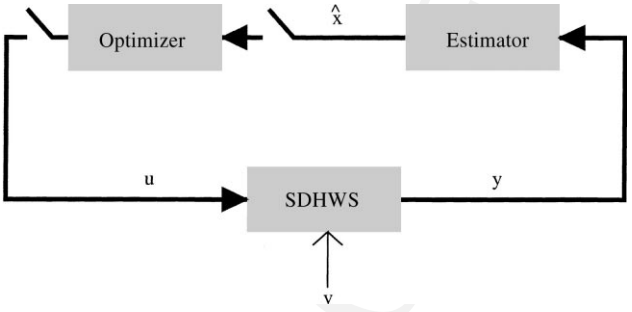


Fig. 5. Scheme of the feedback mechanism.

The complete feedback mechanism is schematized in Fig. 5.

6. State estimator based on an extended Kalman filter

The estimator chosen in this work is an extended Kalman filter. As a preamble to its description, the discrete linear Kalman filter is reviewed.

The dynamic behavior of the system for which the state vector has to be estimated is described by Eq. (13). The output equation is described by Eq. (14).

$$x(k+1) = A(k)x(k) + w(k) \tag{13}$$

$$y(k) = C(k)x(k) + z(k) \tag{14}$$

where $A(k)$ and $C(k)$ are known matrices with appropriate dimensions.

The noises $w(k)$ and $z(k)$ are independent, zero mean, Gaussian with covariances given by Eqs. (15) and (16).

$$E[w(k)w(l)] = Q(k)\delta_{kl} \tag{15}$$

$$E[z(k)z(l)] = R(k)\delta_{kl} \tag{16}$$

for all k and l, where δ_{kl} is the Kronecker delta, which is 1 for $k = l$ and 0 otherwise.

Suppose that the initial state x_0 is a Gaussian random variable with mean $\overline{x}_0$ and covariance P_0, independent of $w(k)$ and $z(k)$. Thus, it can be proven easily that $x(k)$ and $y(k)$ are Gaussian random variables.

The filtering problem is to estimate $x(k)$ using measurements up to k. This reduces to the computation of the sequence $E[x(k)|y(0), y(1), \ldots, y(k)]$ for $k = 0, 1, 2, \ldots$. This quantity is called $\hat{x}_{k|k}$. It implies the computation of the quantity $E[x(k)|y(0), y(1), \ldots, y(k-1)]$ for $k = 0, 1, \ldots$. This quantity is denoted $\hat{x}_{k|k-1}$. The associated covariance matrices $\Sigma_{k|k}$ and $\Sigma_{k|k-1}$ must also be calculated.

UNCORRECTED PROOF

$\hat{x}_{k|k}$ is the conditional mean estimate, but it has been proven that it is also the minimum variance estimate and the conditional minimum variance estimate, at least with this linear discrete system and with the assumptions on the noises aforementioned.

The solution of this filtering problem is now given. The proofs can be found in [7].

- Measurement-update equations:

$$\hat{x}_{k|k} = \hat{x}_{k|k-1} + K(K)[y(k) - C(k)\hat{x}_{k|k-1}] \tag{17}$$

$$K(k) = \Sigma_{k|k-1}C^{\mathrm{T}}(k)[C(k)\Sigma_{k|k-1}C^{\mathrm{T}}(k) + R(k)]^{-1} \tag{18}$$

The matrix $K(k)$ is called the gain of the Kalman filter.

$$\Sigma_{k|k} = [I - K(k)C(k)]\Sigma_{k|k-1} \tag{19}$$

- Time-update equations:

$$\hat{x}_{k+1|k} = A(k)\hat{x}_{k|k} \tag{20}$$

$$\Sigma_{k+1|k} = A(k)\Sigma_{k|k}A^{\mathrm{T}}(k) + Q(k) \tag{21}$$

- Initial conditions:

$$\hat{x}_{k_0|k_0-1} = \overline{x}_0 \tag{22}$$

$$\Sigma_{k_0|k_0-1} = P_0 \tag{23}$$

These equations can be implemented easily. The main difficulty related to this filter lies in the fact that a lot of parameters must be chosen. The matrix R defines the quality of the measurements. This matrix is often chosen diagonal. If the ith measurement is good, the ith element of the diagonal of R must be small. The Q matrix is also chosen diagonal, each element of this diagonal defines the quality of the corresponding differential equation. For example, if it is clear that the ith equation is very close to reality then the ith element of the diagonal of Q must be small. The opposite is true. $\overline{x}_0$ is roughly evaluated owing to the measurements taken at k_0, and P_0 is chosen diagonal. The elements of this diagonal are the tuning parameters for the filter convergence.

As mentioned above, an extended version of the Kalman filter has to be used for the SDHWS. The differential equations of the model of the system are neither linear nor discrete. They are given by

$$\dot{x}(t) = f[x(t), u(t), p, v(t)] + w(t) \tag{24}$$

The output equation is still linear and given by

$$y(t_k) = Cx(t_k) + z(t_k) \tag{25}$$

This equation shows that the measurements are taken at discrete times t_k, every 10 min in our special case.

The assumptions on the noises w and z are the same as in the linear-discrete case.

This model must be linearized around a nominal trajectory which is not known in advance. The solution is called the prediction-correction method. The nominal state $\overline{x} = \hat{x}(t|t_k)$ in the interval $[t_k, t_{k+1})$ is obtained by integrating numerically the following system of non-linear differential equations:

$$\overline{\dot{x}}(t|t_k) = f[\hat{x}(t|t_k), \overline{u}(t), p, \overline{v}(t)] \tag{26}$$

Thus, from t_k to t_{k+1}, starting from the initial condition $\hat{x}(t_k|t_k)$, this numerical integration provides $\hat{x}(t_{k+1}, t_k)$. From this, the nominal trajectory of the output is obtained easily owing to

$$\overline{y}(t_{k+1}, t_k) = C\hat{x}(t_{k+1}, t_k) \tag{27}$$

Given the nominal trajectory, the Jacobian matrix can be computed the following way:

$$F(t|t_k) = F[\hat{x}(t|t_k), u(t), v(t)] = \left.\frac{\delta f[x(t), u(t), p, v(t)]}{\delta x}\right|_{x=\hat{x}(t|t_k)} \tag{28}$$

The equations of the extended Kalman filter are given by

- Measurement-update equations (correction):

$$K(t_k) = \Sigma(t_k|t_{k-1})C^{\mathrm{T}}[C\Sigma(t_k|t_{k-1})C^{\mathrm{T}} + R)]^{-1} \tag{29}$$

$$\hat{x}(t_k|t_k) = \hat{x}(t_k|t_{k-1}) + K(t_k)[y(t_k) - C\hat{x}(t_k|t_{k-1})] \tag{30}$$

$$\Sigma(t_k|t_k) = [I - K(t_k)C]\Sigma(t_k|t_{k-1}) \tag{31}$$

- Time-update equations (prediction):

$$\dot{\hat{x}} = f[\hat{x}(t|t_k), u(t), p, v(t)] \tag{32}$$

$$\dot{\Sigma}(t|t_k) = F[\hat{x}(t|t_k), u(t), v(t)]\Sigma(t|t_k) + \Sigma(t|t_k)F^{\mathrm{T}}[\hat{x}(t|t_k), u(t), v(t)] + Q \tag{33}$$

- Initial conditions:

$$\hat{x}(t_1|t_0) = \overline{x}_0 \tag{34}$$

$$\Sigma(t_1|t_0) = P_0 \tag{35}$$

Time-update equations are numerically solved from t_k to t_{k+1}. The parameters of this filter are the same as in the linear-discrete case and are tuned in the same way.

The prediction is computed each time new measurements are taken, every 10 min. The optimization procedure could also be repeated every 10 min if there is enough time. However, in our special case, the optimization is not performed so often. The innovation sequence $\mathrm{Inov}(t_k)$ is used to decide whether a new optimization should be performed. It is defined as follows:

$$\mathrm{Inov}(t_k) = \hat{x}(t_k|t_k) - \hat{x}(t_k|t_{k-1}) \tag{36}$$

Usually, all the elements of the vector $\mathrm{Inov}(t_k)$ are small. If one of them is bigger than a predefined constant, it means that either the model has failed to predict the behavior of the SDHWS or the disturbances (weather data or users' needs in terms of draw-off) have been badly estimated. In both cases, the optimization has to be performed to tackle this problem.

In our special case, $\mathrm{Inov}(t_k)$ is a 28-dimensional vector, and its elements represent a difference of temperatures for a

UNCORRECTED PROOF

given node of the model. Thus, the optimization is repeated each time one of the element of $\mathrm{Inov}(t_k)$ is greater than a few degrees Kelvin (or Celsius).

7. Weather forecasts and prediction of the users' needs

It is obvious that the model is not sufficient to predict the behavior of the SDHWS. The solar radiation, the ambient temperature around the collector and the users' needs in terms of draw-off must be predicted. The temperature of the water at the input of the storage tank as well as the ambient temperature around the storage tank does not have to be predicted. Their influence is not significant and they can be chosen constant over H.

As for the weather forecasts, stochastic models can be built [8]. However, the Swiss Meteorological Institute (SMI) is able to provide via e-mail accurate 2-day forecasts. An advanced model is used to compute these forecasts. It describes all of the relevant atmospheric phenomena at different scales, like storms, wind, rain, high clouds, snow, etc. Obviously, we could not have afforded to create such a huge model ourselves because of computational limitations.

With regards to the users' needs in terms of draw-off, the tapped water predicted for each day of the week is the average of the corresponding day over the last two months. This prediction is updated every day at midnight.

The main problem is the fact that a flow meter is too expensive to consider for measuring the flow rate of the tapped water. Therefore, the extended Kalman filter described in the previous section is also used to fulfill this task.

For that purpose, the dimension of the state vector x is increased by one. This new state vector is called x_c. The new element is the disturbance that has to be estimated. In this case, it is the flow rate of the tapped water $\dot{m}_L$. Below, it matches the ith disturbance v_i. To apply the equations of the extended Kalman filter, the dynamics of this disturbance v_i is defined as

$$\frac{\mathrm{d}v_i}{\mathrm{d}t}(t) = f_{v_i} v_i(t) + n_{v_i}(t) \tag{37}$$

Thus, this differential equation together with the 28 others of the model of the SDHWS lead to the following general representation:

$$\dot{x}_c(t) = f_c[x_c(t, u(t), p, v(t)] + w_c(t) \tag{38}$$

The dimension of the vector w has also been increased by one. The 28 first elements of the vector w_c correspond to the elements of w. The last element is n_{v_i}. The assumptions on this new element are the same as the others. The output equation remains unchanged. With this new model, the procedure used is exactly the same as the one described for the extended Kalman filter in the previous section (just replace x by x_c and adapt the dimensions of the various functions accordingly).

There are some new parameters that have to be defined to make this filter work properly. First, the dynamics of the estimated disturbance f_{v_i} must be defined. In fact, the dynamics of this disturbance is not known in advance. It is chosen to equal zero. However, owing to the noise n_{v_i}, it can be indicated easily to the filter that this dynamics is not known. This is done by choosing a high value for the corresponding term in the diagonal of the covariance matrix Q.

Finally, initial conditions for this disturbance v_i and its covariance are given. Both are taken as equal to zero.

A flow meter has been installed in a pilot plant to compare the flow rate measured with the one estimated by the filter. A typical result for this comparison is shown in Fig. 6. The filter has no a priori knowledge of the tapped-water profile we have imposed. The profile chosen is standardized to validate the SDHWS. Even if its shape may be different from a measured one, it exhibits all the discontinuities necessary to validate the filter.

Therefore, the users' needs in terms of draw-off are well evaluated on-line owing to this filter. As mentioned above, this estimation is used at the end of the day to update the prediction used in the optimization procedure.

8. Control strategies validation

This section presents simulation results that illustrate the performances of the various strategies applied to control a modified or a conventional SDHWS.

Comparison criteria have to be defined to assess the energy performance improvement of this advanced control strategy coupled to the segmented auxiliary heater. The energy balance of the SDHWS is given by

$$E_{\mathrm{elec}} + E_{\mathrm{sol}} = E_{\mathrm{load}} + E_{\mathrm{amb}} + \Delta E \tag{39}$$

with

$$E_{\mathrm{elec}} = \int_B P_{\mathrm{elec}}\,\mathrm{d}t = \int_B (P_1 + P_2 + P_3)\,\mathrm{d}t \tag{40}$$

$$E_{\mathrm{sol}} = \int_B P_{\mathrm{sol}}\,\mathrm{d}t = \int_B \dot{m}_{\mathrm{C}} C_{pc}(T_{p,3} - T_{p,2})\,\mathrm{d}t \tag{41}$$

$$E_{\mathrm{load}} = \int_B \dot{m}_{\mathrm{L}} C_{pf}(T_{s,1} - T_{\mathrm{in}})\,\mathrm{d}t \tag{42}$$

The horizon B over which these integrals are specified is the horizon chosen to compare the two configurations.

E_{elec} is the electrical energy consumed and E_{sol} is the solar energy gathered. E_{load}, E_{amb} and ΔE are the energy tapped by the users, the ambient energy loss and the variation of the internal energy of the SDHWS, respectively. This last term depends on the temperature variation of the 28 nodes over the B horizon.

UNCORRECTED PROOF

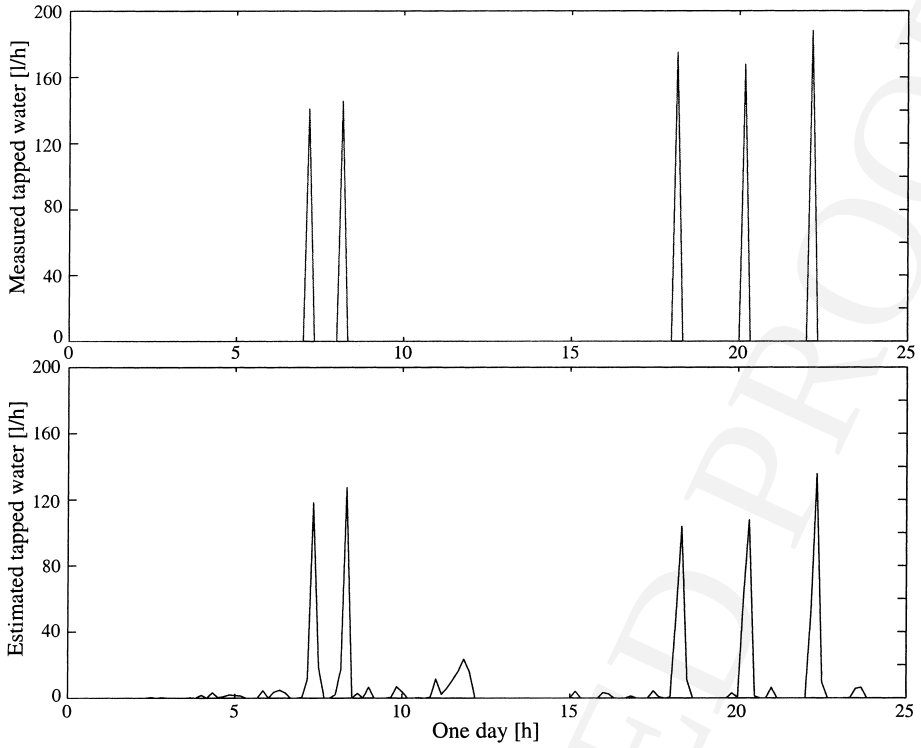


Fig. 6. Comparison between measured and estimated tapped water.

Two criteria F_1 and F_2 have been chosen. They are often referred to as the solar fraction:

$$F_1 = \frac{E_{sol}}{E_{load} + E_{amb}} = \frac{E_{sol}}{E_{sol} + E_{elec} - \Delta E} \quad (43)$$

$$F_2 = \frac{E_{sol}}{E_{load}} = \frac{E_{sol}}{E_{sol} + E_{elec} - \Delta E - E_{amb}} \quad (44)$$

F_1 is obviously lower than F_2. F_1 penalizes the strategies that lead to a great amount of ambient energy loss. Therefore, even if F_2 is used commonly, it seems that F_1 is more representative of the quality of a configuration.

The first part of this section justifies the choice of an on–off power supply for the modified SDHWS that integrates a segmented auxiliary heater.

With this choice, the second part of the section quantifies the benefit of such a modified SDHWS compared to the traditional one that integrates a unique auxiliary heater. The energy performance improvements presented in this section suppose that there are no model mismatches and that the disturbances are perfectly predicted. In a real situation, these conditions may not be well satisfied. The implications of the resulting discrepancies in the users' behavior and in the weather forecasts will be discussed in Section 9.

8.1. Power supply alternative for the modified SDHWS

First, it is assumed that the electrical elements can be supplied continuously. The long, the medium, and the short electrical element can afford power supplies of 1.5, 1.0, and 0.5 kW, respectively. Thus, all of the inputs are chosen piecewise continuous functions with a period equal to two times the sampling rate. This leads to 288 decision variables over a 1-day horizon (4 inputs times 72 decision variables per input).

Curves in Fig. 7 exhibit the profiles of the solar radiation chosen to carry out the simulation and the corresponding optimal flow rate provided by the optimization procedure.

In Fig. 8, the profile of the water tapped and the corresponding continuous optimal power supply of each electrical element are shown. Owing to the predictive behavior of the controller, the auxiliary heaters are used mainly just before water is tapped. In this simulation, the amount of water tapped is low. Thus, the longest electrical element is almost never used. This proves the benefit of the segmented auxiliary heater.

These results also suggest that it may not be necessary to power continuously the auxiliary heaters. The shape of the continuous optimal solution is close to an on–off sequence. Thus, a sub-optimal solution can be obtained with less computational load by looking for an on–off sequence with a predefined number of switching times. The simulation has been carried out and the results are shown in Fig. 9.

The general behavior is almost the same, the auxiliary heaters are turned on just before the water is tapped and the third electrical element is not used. All the elements of the energy balance previously defined have been computed for the 1-day period considered and can be seen in Table 1. In terms of solar fraction, the performances are approximately the same in both the continuous and on–off cases.

UNCORRECTED PROOF

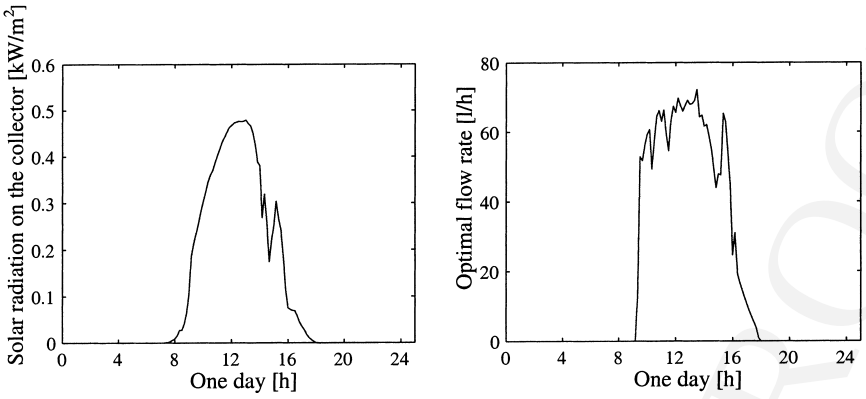


Fig. 7. Solar radiation and optimal flow rate.

Temperature profiles inside the storage tank are shown in Fig. 10. The degree of comfort is very high in both cases, since the temperature in the upper part of the storage tank stays close to the set temperature T_{set} of 55°C.

8.2. Advanced control strategy versus conventional one

From now on, it is considered that an on–off power supply of the auxiliary heaters is implemented.

The conventional strategy for the SDHWS under consideration is the following:

$P_1 = 0$

$P_2 = 0$

$P_3 = 3.0\,\text{kW} \quad \text{if}(M_1 + M_2 + M_3) < 55°\text{C}$

$P_3 = 0.0\,\text{kW} \quad \text{if}(M_1 + M_2 + M_3) > 55°\text{C}$

P_1 and P_2 are equal to zero because there is only the largest electrical element in the conventional configuration. It can afford a 3.0 kW power supply. It corresponds to the same total power affordable as the configuration with the segmented auxiliary heater. M_1, M_2 and M_3 are the three temperature measurements located in the upper part of the storage tank (see Fig 1). The set temperature for this conventional strategy has been chosen 55°C in order to ease the comparison with our advanced control strategy and its T_{set}, also equal to 55°C.

The simulation has been carried out over a 28-day horizon. It is enough to reduce the influence of the variation of the internal energy and also enough to cover a wide spectrum of operational conditions (weather data and users' needs in terms of draw-off). For conciseness, profiles of the water tapped and meteorological

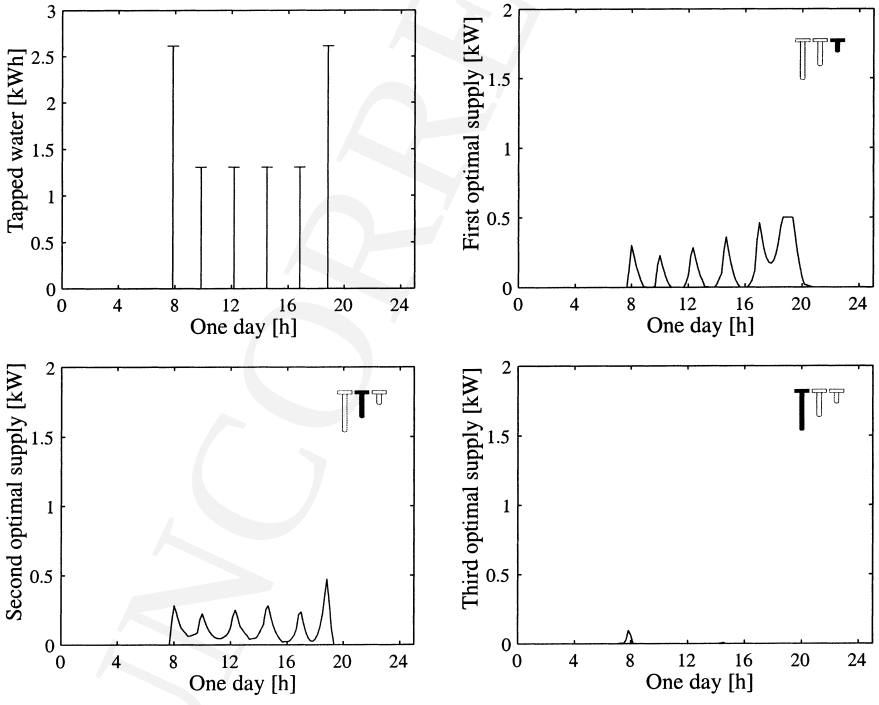


Fig. 8. Tapped water and continuous optimal power supply of each auxiliary heater.

UNCORRECTED PROOF

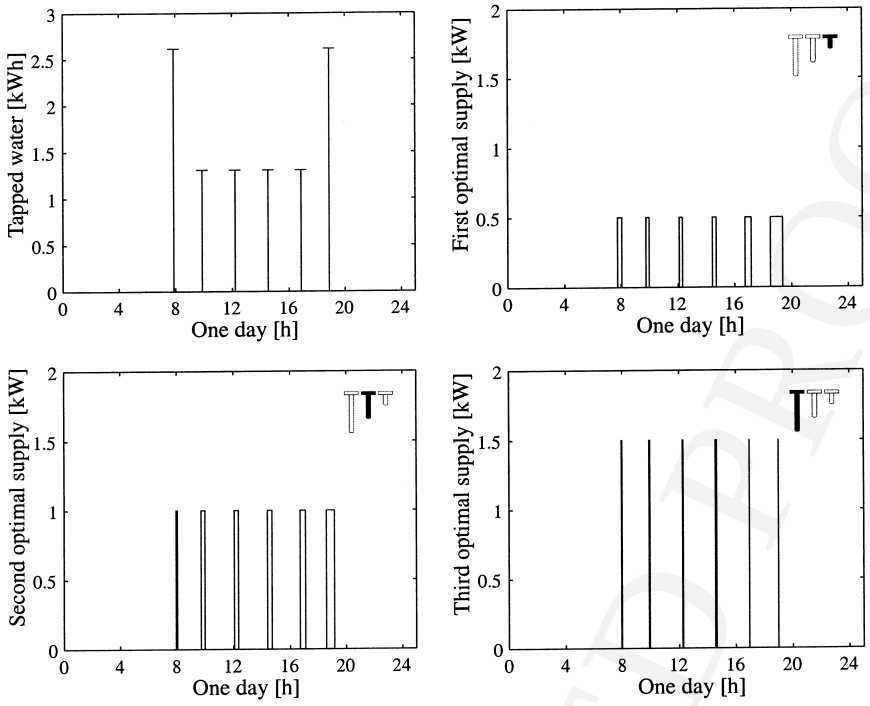


Fig. 9. Tapped water and on–off optimal power supply of each auxiliary heater.

Table 1
Comparison between continuous and on–off power supply in terms of energy performances

	Continuous power supply	On–off power supply	Variation (%)
E_{elec} (kJ)	3.69*e*4	3.73*e*4	+1.08
E_{sol} (kJ)	2.63*e*4	2.63*e*4	0.00
E_{amb} (kJ)	6.57*e*3	6.79*e*3	+3.3
ΔE (kJ)	1.53*e*3	1.71*e*3	−11.76
E_{load} (kJ)	5.51*e*4	5.51*e*4	0.00
F_1 (%)	42.64	42.49	+0.35
F_2 (%)	47.73	47.73	0.00

data are not given. They are identical for the two configurations.

On the left-hand side of Fig. 11, the temperatures of the 13 nodes of the SDHWS model for the 28th day resulting from the new configuration are shown. On the right-hand side, the temperatures for the same day resulting from the conventional configuration are shown.

All the elements of the energy balance have been computed for the 28-day period and are shown in Table 2.

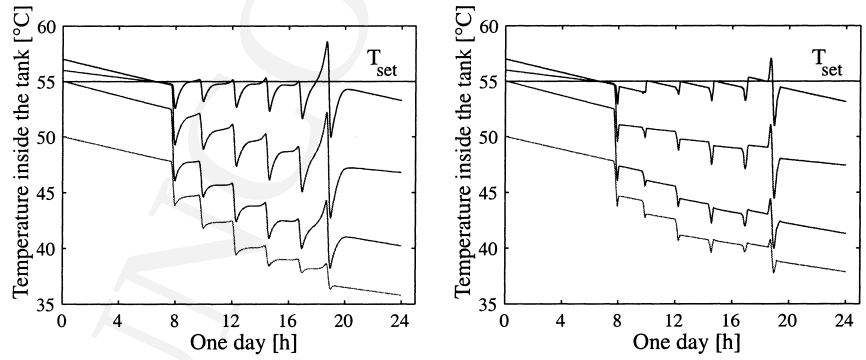


Fig. 10. Left: continuous power supply; right: on–off power supply.

UNCORRECTED PROOF

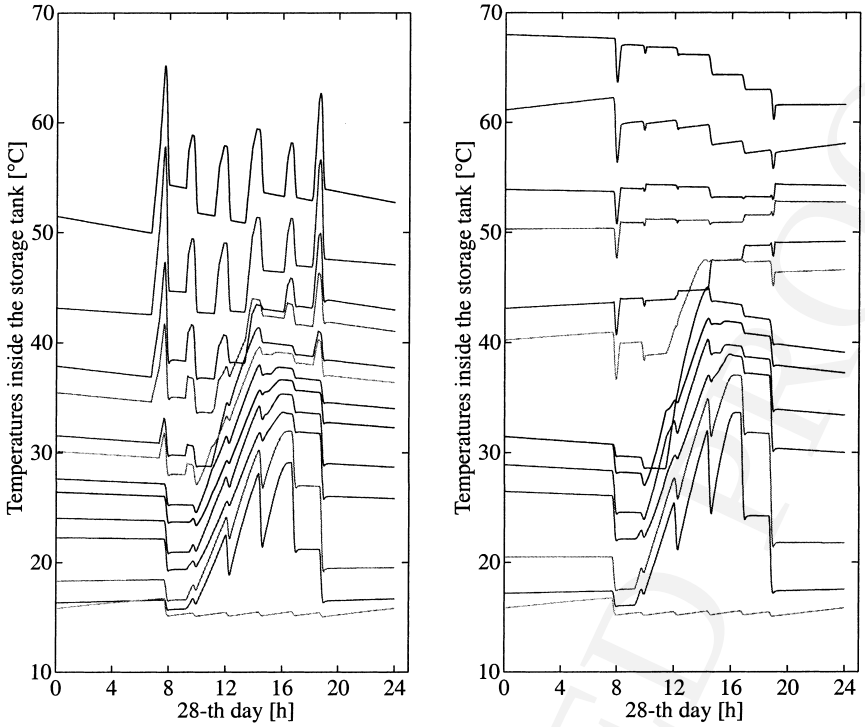


Fig. 11. Left: new configuration; right: conventional configuration

From the conventional configuration compared to the new one, E_{elec} has been reduced by 10.0%. This decrease is due to both a decrease of E_{amb} and an increase of E_{sol}. It results from the fact that the mean temperature inside the storage tank is lower in the new configuration. This can be seen clearly in Fig. 11. It should be noted that the mean temperature in the conventional configuration is highly dependent on the chosen T_{set}. The value chosen to carry out these simulations is the same for the two configurations. However, in the current practice, the value chosen is higher than 55°C for the conventional control strategy. Indeed, the temperature in the storage tank has to be high enough to prevent the biggest peak of tapped water with the worst weather. With the advanced control strategy proposed, a lower T_{set} can be afforded because estimations of the users' needs and forecasts of the most significant weather data are taken into account explicitly. Thus, it gives the anticipation effect necessary allowing a lower mean temperature in the storage tank.

9. Concluding remarks

An advanced control strategy coupled with a segmented auxiliary heater have led to a significant increase of the solar fraction and a higher degree of comfort. Electrical elements do not have to be continuously powered. Moreover, an on–off control strategy is also more suitable from a computational point of view. Indeed, this optimization can be achieved in a fraction of the 10 min sampling period.

However, as already mentioned, these are simulation results. In practice, they would be dependent on the quality of the disturbances' estimates. However, this problem is partly tackled by the fact that the optimization is repeated

Table 2
Energy balances

	Conventional configuration	New configuration	Variation (%)
E_{elec} (kJ)	1.02*e*6	9.17*e*5	−10.5
E_{sol} (kJ)	7.36*e*5	7.76*e*5	+5.50
E_{amb} (kJ)	1.88*e*5	1.33*e*5	−29.4
ΔE (kJ)	2.43*e*4	1.23*e*4	−49.6
E_{load} (kJ)	1.55*e*6	1.55*e*6	0.00
F_1 (%)	42.4	46.2	+8.94
F_2 (%)	47.5	50.1	+5.47

UNCORRECTED PROOF

frequently. Indeed, each time new measurements are available, the state estimator computes new initial conditions for the optimization algorithm which is therefore able to provide updated optimal inputs. It will fail only in the case of real disturbances very different from their estimates. In that case, another degree of robustness is necessary. For example, rather than keeping only the temperature of the highest node in the storage tank close to T_{set}, it may be specified to the optimizer to keep the temperature of two or more nodes in the storage tank close to this same T_{set}. It would assure a given amount of energy in reserve in case of under-estimated draw-off or over-estimated solar radiation. Thus, the objective function would be:

$$J = \int_{\text{one day}} \{[P_{\text{elec}} - (P_{\text{sol}} - P_{\text{pump}})] + \alpha_1 (T_{s,1} - T_{\text{set}})^2 + \alpha_2 (T_{s,2} - T_{\text{set}})^2\} \, \mathrm{d}t$$

To conclude, the control strategy has to be conservative enough depending on the quality of the estimates. On one hand, if the estimates are very good, the control strategy would not be too conservative and the energy performances will be excellent. On the other hand, if no a priori knowledge of these disturbances is available, it will be difficult to get better performances than the conventional control strategy.

As for commercial applications, it may be difficult to consider getting information such as weather forecasts at every SDHWS because it requires communication capabilities. Moreover, the advanced control strategy is based on the solving of a complex optimization problem that necessitates significant computation capabilities. However, there is no doubt that these two points won't be problematic in the near future and the energetic benefits induced by the new configuration will fully justify the price of the modifications.

Acknowledgements

This work is supported by the Swiss Federal Office of Energy, Grant DIS 22260.

References

[1] T. Prud'homme, D. Gillet, Optimisation of solar domestic hot water systems, in: EuroSun'98, Portorož, Slovenia, Vol. 2, 1998.
[2] S.J. Qin, T.A. Badgwell, An overview of Industrial model predictive control technology, in: J.C. Kantor, C.E. Garcia, B. Carnahan (Eds.), Fifth International Conferences on Chemical Process Control, CACHE, AICHE, 1997, pp. 232–256.
[3] Y. Oestreicher, M. Bauer, J.-L. Scartezzini, Accounting free gains in a non-residential building by means of an optimal stochastic controller, Energy Building 24 (3) (1996) 213–221.
[4] I.R. Williamsons, S. Danaher, C. Craggs, Optimisation of solar building control using predictive methodologies, in: 6th European Congress on Intelligent Techniques and Soft Computing, EUFIT'98, Vol. 2, Verlag Mainz, Aachen, Germany, 1998, pp. 878–879.
[5] E.F. Camacho, M. Berenguel, F.R. Rubio, Application of a gain scheduling generalized predictive controller to a solar power plant, Control Eng. Practice 2 (1994) 227–238.
[6] G. Luenberger, Linear and Nonlinear Programming, Addison-Wesley, Reading, MA, 1984.
[7] B.D.O. Anderson, J.B. Moore, Optimal Filtering, Prentice-Hall, Englewood Cliffs, NJ, 1979.
[8] J.-L. Scartezzini, Application des méthodes stochastiques à l'étude des systèmes de catage de l'énergie solaire, Ph.D. Thesis, École Polytechnique Fédérale de Lausanne, 1986.

UNCORRECTED PROOF